Chinese Chemical Letters 32 (2021) 2769–2772

Contents lists available at ScienceDirect

Chinese Chemical Letters

journal homepage: www.elsevier.com/locate/cclet

Communication

Origins of catalyst-controlled enantiodivergent hydroamination of enones with pyridazinones: A computational study

Xiangwei Ren[1], Hongli Wu[1], Mei Zhang, Wentao Zhao*, Genping Huang*

Department of Chemistry, School of Science and Tianjin Key Laboratory of Molecular Optoelectronic Sciences, Tianjin University, Tianjin 300072, China

ARTICLE INFO

Article history:
Received 15 January 2021
Received in revised form 22 February 2021
Accepted 23 February 2021
Available online 25 February 2021

Keywords:
Dipeptide phosphine catalyst
Hydroamination
Mechanism
Selectivity
DFT calculations

ABSTRACT

Density functional theory calculations have been performed to investigate the dipeptide phosphine-catalyzed hydroamination of enones with pyridazinones. The computations reveal that a number of the N—H···O hydrogen-bonding interactions with the pyridazinone moiety and the C–H···O hydrogen-bonding interactions with the enone moiety are present in the enantioselectivity-determining Michael addition transition states. The experimentally-observed catalyst-controlled enantiodivergence is mainly attributed to the significant impact of the substituent of the amide moiety of the dipeptide phosphine on the relative strength of the N—H···O hydrogen-bonding interactions, which was found to affect the *Si* face attack transition state, enabling the enantioselectivity switch upon change of chiral dipeptide phosphine catalyst.

The organocatalyzed reactions for the asymmetric synthesis of C—C and C–X bonds have gained extensive research interest in organic chemistry, which provide a complementary strategy to the metal- and enzyme-catalyzed reactions [1,2]. Over past decades, a wide range of the organocatalysis, such as Brønsted acids, phosphines, *N*-heterocyclic carbenes, prolines and thiourea catalysts, has been developed [2]. In this respect, considerable research efforts have been devoted to the phosphine catalysts, which have shown great potential for the cycloaddition and addition reactions [3]. For instance, Trost and co-workers in 1994 developed the phosphine-catalyzed "umpolung" addition [4]. Lu and co-workers in 1995 reported an early discovery on the phosphine-catalyzed [3 + 2] annulation between 2,3-butadienoates or 2-butynoates with electron-deficient olefins [5], which has become one of the most powerful tools for the construction of the five-membered-ring carbo- and heterocycles.

Despite the significance progress has been witnessed, the development of the enantiodivergent phosphine-catalyzed reactions remains a central challenge in this field [6]. In this context, Zhang and co-workers very recently reported an elegant example of the dipeptide phosphine-catalyzed hydroamination of enones **2** with pyridazinones **1** (Scheme 1) in high yields and with good enantioselectivity [7]. The salient feature of the reaction is that both enantiomers of the addition products **3** can be obtained by the careful selection of the dipeptide phosphine catalyst. It was found that with the dipeptide phosphine **P1**, the addition of pyridazinones **1** to enones **2** can give the products (*R*)-**3** with the excellent enantioselectivity up to 97% *ee*. However, by using the catalyst **P2**, wherein the substituent of the amide moiety of **P1** was changed from the OBoc group to the 3,5-dinitrobenzyl group, the reversed enantioselectivity was observed and the products (*S*)-**3** were obtained with the enantioselectivity up to 99% *ee*. The reaction represents thus a rare case of the enantiodivergent phosphine-catalyzed reactions without changing any stereocenter of the catalyst.

To gain insight into the detailed reaction mechanism and the origins of this unprecedented catalyst-controlled enantioselectivity, density functional theory (DFT) calculations at the M06-2X/6-311+G(*d*,*p*)-SMD//M06-2X/6-31G(*d*)-SMD level of theory were performed (see Supporting information for computational details) [8,9]. The experimentally used β-trifluoromethylated enone **1a** and pyridazinone **2a** were selected as the model substrates. Based on our computational study, the detailed reaction mechanism of the phosphine-catalyzed hydroamination is shown in Scheme 2. The reaction begins with the nucleophilic attack of the phosphine catalyst to methyl acrylate, delivering a zwitterionic intermediate **INT1**, which then undergoes the protonation with pyridazinone **2** to give ionic pair intermediate **INT2**. The subsequent Michael addition between **INT2** and enone **1** leads to intermediate **INT3**. Finally, the catalytic cycle is closed by the protonation of

* Corresponding authors.
E-mail addresses: wentao_zhao@tju.edu.cn (W. Zhao), gphuang@tju.edu.cn (G. Huang).
[1] These authors contributed equally to this work.

https://doi.org/10.1016/j.cclet.2021.02.049

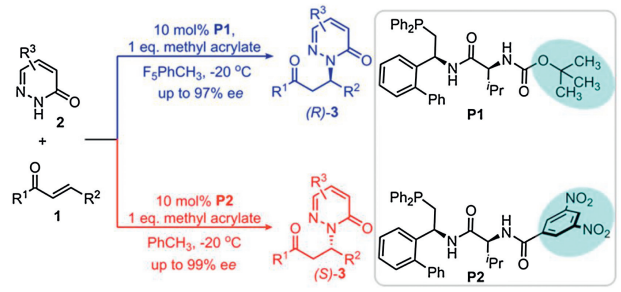

Scheme 1. Dipeptide phosphine-catalyzed enantiodivergent hydroamination reaction.

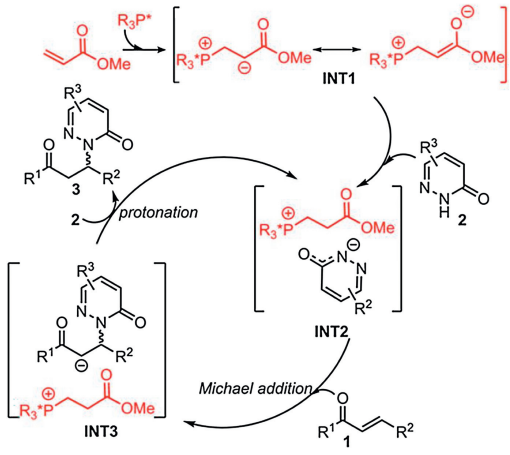

Scheme 2. Proposed reaction mechanism based on DFT calculations.

intermediate **INT3** with pyridazinone **2** to release the hydroamination product **3** and regenerate **INT2**. The computations show that in both **P1**- and **P2**-catalyzed reactions, the Michael addition constitutes the enantioselectivity-determining step of the overall catalytic cycle.

The calculated energy profile of the **P1**-catalyzed reaction is given in Fig. 1a (see Supporting information for the optimized geometries of the selected transition states). The computations show that the nucleophilic attack of the P atom of the catalyst to the methyl acrylate takes place *via* transition state **P1-TS1** with an energy barrier of 16.6 kcal/mol, generating zwitterionic intermediate **P1-INT1**. Then, this intermediate undergoes the protonation with pyridazinone **2a** *via* transition state **P1-TS2** leading to ionic pair intermediate **P1-INT2**. Upon formation of **P1-INT2**, two possible modes of the Michael addition, namely attack of the *Re* and *Si* faces of enone **1a**, were both considered, which were found to occur *via* transition states **P1-TS3-*Re*** and **P1-TS3-*Si***, respectively. Finally, the protonation of the resulting intermediates **P1-INT3-*Re*** and **P1-INT3-*Si*** with pyridazinone **2a** to regenerate **P1-INT2** and release the hydroamination products (*R*)-**3a** and (*S*)-**3a**, respectively. The results show that the *Re* face attack through transition state **P1-TS3-*Re*** is lower in energy than the *Si* face attack *via* transition state **P1-TS3-*Si*** by 2.7 kcal/mol, which is in good agreement with the experimentally observed 95% *ee* in favor of (*R*)-**3a**.

The **P2**-catalyzed reaction follows the same reaction mechanism as established for the case of the **P1** catalyst (Fig. 1b and see Supporting information for the optimized geometries of the selected transition states). However, the catalyst was indeed found to have a significant impact on switching the enantioselectivity. With the **P2** catalyst, the *Re* face attack *via* transition state **P2-TS3-*Re*** is disfavored over the *Si* face attack *via* transition state **P2-TS3-*Si*** by 2.9 kcal/mol, being in accordance with the experiments that the reversed enantioselectivity was observed for the **P2**-catalyzed reaction. Therefore, the calculations reproduced quite well the experimentally observed catalyst-controlled enantioselectivity.

The optimized geometries of the enantioselectivity-determining transition states are given in Fig. 2. The computations show that a number of the N—H···O hydrogen-bonding interactions with the pyridazinone moiety and the C–H···O hydrogen-bonding interactions with the β-trifluoromethylated enone moiety are present in enantioselectivity-determining Michael addition transition states. For the **P1**-catalyzed reaction, the distortion/interaction analysis [10] of **P1-TS3-*Si*** and **P1-TS3-*Re*** was conducted to gain insights into the origins of the selectivity. As depicted in Table 1, the results show that the distortion energies of **1a** ($\Delta E_{\mathbf{1a}}$) for both transition states are nearly identical (4.9 and 4.1 kcal/mol). The selectivity is mainly determined by the difference in the distortion energy of **P1-INT2**. $\Delta E_{\mathbf{P1\text{-}INT2}}$ of **P1-TS3-*Si*** was calculated to be higher than that of **P1-TS3-*Re*** by 3.5 kcal/mol (8.2 kcal/mol *versus* 4.7 kcal/mol), which consequently results in the energy of **P1-TS3-*Si*** being higher than **P1-TS3-*Re***. The origins of this is likely due to that for the *Si* face attack, the pyridazinone moiety of **P1-INT2** has to be distorted to achieve the geometric structure of the **P1-TS3-*Si***. On the other hand, the relative orientation of the pyridazinone moiety can readily undergo the *Re* face attack.

By changing the catalyst to **P2**, the geometric structure of the *Re* face attack transition state **P2-TS3-*Re*** was found to be quite different to that of **P1**. We have also considered the *Re* face attack transition state with **P2** with the geometric structure similar to that of **P1-TS3-*Re***. However, due to the steric repulsion between the 3,5-dinitrobenzyl group and pyridazinone, the energy of the corresponding transition state was calculated to be 2.8 kcal/mol higher in energy than **P2-TS3-*Re*** (see Supporting information for details). The comparison of the optimized geometries of **P1-TS3-*Si*** and **P2-TS3-*Si*** shows that the substituent of the amide moiety has a significant impact on the relative strength of the N—H···O hydrogen-bonding interactions. In **P1-TS3-*Si***, the N—H···O hydrogen-bonding interaction a1 is weaker than a2 (1.93 Å *versus* 1.77 Å and E_{NBO} = 8.41 kcal/mol of a1 *versus* E_{NBO} = 15.52 kcal/mol of a2). While in **P2-TS3-*Si***, due to the strong electron-withdrawing character of the 3,5-dinitrobenzyl group, the N—H···O hydrogen-bonding interaction a1 was found to be slightly stronger than a2 (1.84 Å *versus* 1.86 Å and E_{NBO} = 13.10 kcal/mol of a1 *versus* E_{NBO} = 10.21 kcal/mol of a2). Very importantly, the difference in the relative strength of the N—H···O hydrogen-bonding interactions makes the orientation of the pyridazinone being quite different in two transition states. In **P1-TS3-*Si***, the pyridazinone was found to orient away from the β-trifluoromethylated enone moiety, where in **P2-TS3-*Si***, the pyridazinone was found to orient toward to the β-trifluoromethylated enone moiety. As a result, the distance of the forming C—N bond in **P2-TS3-*Si*** was found to be much shorter than in **P1-TS3-*Si*** (2.14 Å *versus* 2.34 Å), which may facilitate the *Si* face attack and thus enable the enantioselectivity switch upon change of chiral dipeptide phosphine catalyst. This argument is also in accordance with the control experiments that the second N2-H of chiral dipeptide phosphine catalyst is crucial to reverse the enantioselectivity [7].

To summarize, we have herein presented a mechanistic study on the dipeptide phosphine-catalyzed hydroamination of enones with pyridazinones by means of DFT calculations. The computations show that the enantioselectivity of the reaction is determined by the Michael addition between enone and the ionic pair intermediate, generated by the initial nucleophilic attack/protonation. The

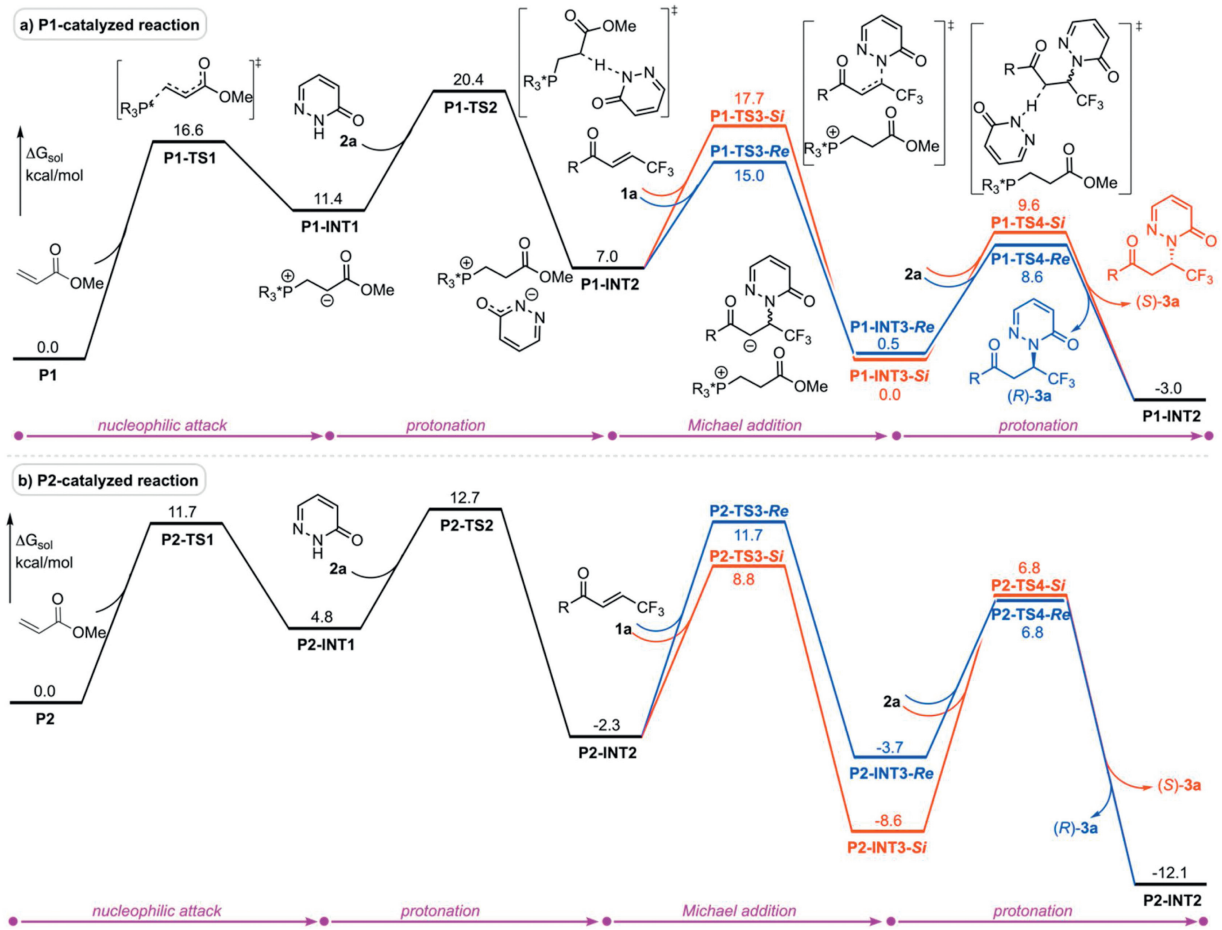

Fig. 1. Calculated energy profiles of the **P1**- and **P2**-catalyzed hydroamination of **1a** with **2a** (R = 4-ClC$_6$H$_4$).

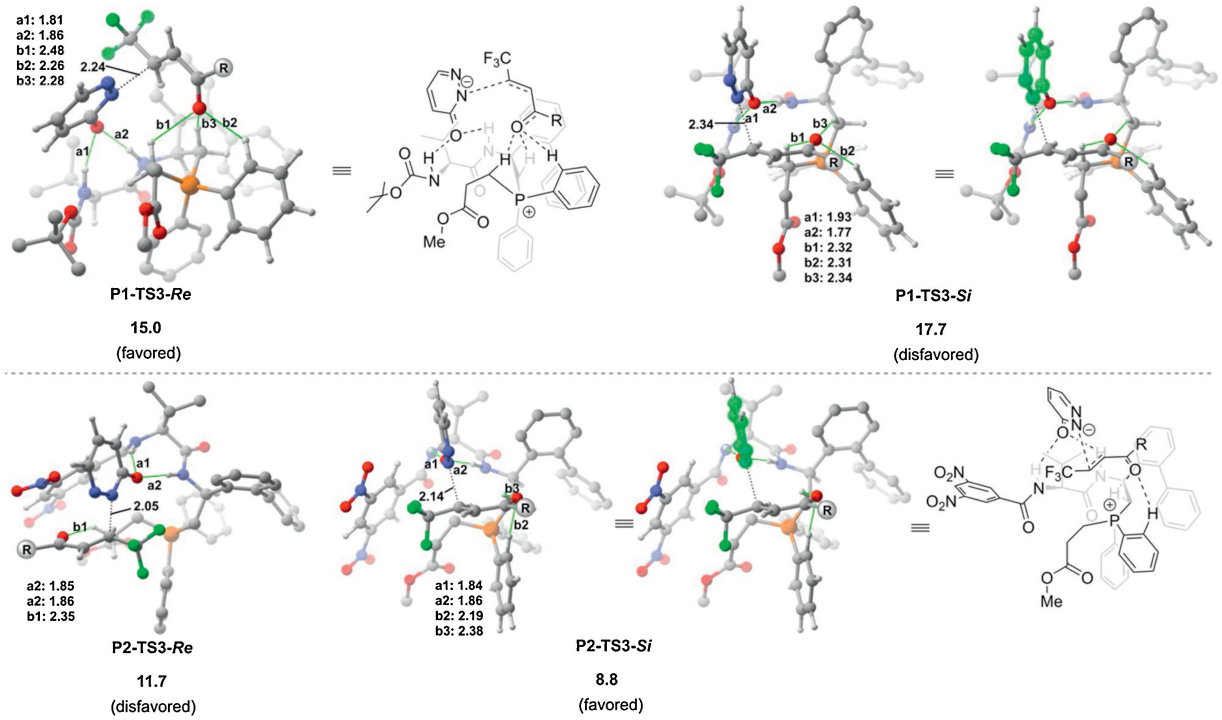

Fig. 2. Optimized geometric structures of the Michael addition transition states (R = 4-ClC$_6$H$_4$). Energies and bond distances are given in kcal/mol and Å, respectively. For the sake of clarity, some irrelevant hydrogen atoms were omitted.

Table 1
Distortion/interaction analysis (kcal/mol) of **P1-TS3-*Si*** and **P1-TS3-*Re***.[a]

TS	$\Delta E_{\mathbf{P1\text{-}INT2}}$	$\Delta E_{\mathbf{1a}}$	ΔE_{int}
P1-TS3-*Si*	4.7	4.9	−17.4
P1-TS3-*Re*	8.2	4.1	−16.3

[a] The distortion/interaction analysis was performed at the level of M06-2X/6-311+G(*d*,*p*)-SMD; $\Delta E_{\mathbf{P1\text{-}INT2}}$ and $\Delta E_{\mathbf{1a}}$ are the energies required to distort the **P1-INT2** and **1a** into the transition state geometries, respectively. The ΔE_{int} is the energy gained by the interaction between the distorted moieties.

experimentally-observed catalyst-controlled enantiodivergence was reproduced quite well by the calculations. It was found that a number of the N—H···O hydrogen-bonding interactions with the pyridazinone moiety and the C–H···O hydrogen-bonding interactions with the *β*-trifluoromethylated enone moiety are present in the Michael addition transition states. The electronic character of the substituent of the amide moiety of the dipeptide phosphine has a significant impact on the relative strength of the N—H···O hydrogen-bonding interactions, which was found to affect the *Si* face attack transition state, leading to the enantioselectivity switch upon change of chiral dipeptide phosphine catalyst.

Declaration of competing interest

The authors declare that they have no known competing financial interests or personal relationships that could have appeared to influence the work reported in this paper.

Acknowledgments

This work was supported by the National Natural Science Foundation of China (Nos. 22073066, 21503143 and 21975179) and the Natural Science Foundation of Tianjin (No. 16JCQNJC05600).

Appendix A. Supplementary data

Supplementary material related to this article can be found, in the online version, at doi:https://doi.org/10.1016/j.cclet.2021.02.049.

References

[1] (a) S. Mukherjee, J.W. Yang, S. Hoffmann, B. List, Chem. Rev. 107 (2007) 5471–5569;
(b) Y. Qin, L. Zhu, S. Luo, Chem. Rev. 117 (2017) 9433–9520;
(c) L. Dai, S. Ye, Chin. Chem. Lett. 32 (2021) 660–667;
(d) E.Z. Lin, Y. Xu, K. Ji, L.W. Ye, Chin. Chem. Lett. 32 (2021) 954–962;
(e) W. Cao, X. Liu, X. Feng, Chin. Chem. Lett. 29 (2018) 1201–1208.
[2] (a) Y.C. Fan, O. Kwon, Chem. Commun. 49 (2013) 11588–11619;
(b) B.J. Cowen, S.J. Miller, Chem. Soc. Rev. 38 (2009) 3102–3116;
(c) H. Guo, Y.C. Fan, Z. Sun, Y. Wu, O. Kwon, Chem. Rev. 118 (2018) 10049–10293;
(d) H. Ni, W.L. Chan, Y. Lu, Chem. Rev. 118 (2018) 9344–9411.
[3] (a) X. Han, W.L. Chan, W. Yao, Y. Wang, Y. Lu, Angew. Chem. Int. Ed. 55 (2016) 6492–6496;
(b) Y. Gu, P. Hu, C. Ni, X. Tong, J. Am. Chem. Soc. 137 (2015) 6400–6406;
(c) B. Huang, C. Li, H. Wang, et al., Org. Lett. 19 (2017) 5102–5105;
(d) W. Zhou, H. Wang, M. Tao, et al., Chem. Sci. 8 (2017) 4660–4665;
(e) W. Yao, Z. Yu, S. Wen, et al., Chem. Sci. 8 (2017) 5196–5200;
(f) H. Ni, Z. Yu, W. Yao, et al., Chem. Sci. 8 (2017) 5699–5704;
(g) J. Zhang, H.H. Wu, J. Zhang, Org. Lett. 19 (2017) 6080–6083;
(h) L. Zhang, H. Liu, G. Qiao, et al., J. Am. Chem. Soc. 137 (2015) 4316–4319;
(i) H. Wang, L. Zhang, Y. Tu, et al., Angew. Chem. Int. Ed. 57 (2018) 15787–15791.
[4] B.M. Trost, C.J. Li, J. Am. Chem. Soc. 116 (1994) 3167–3168.
[5] C. Zhang, X. Lu, J. Org. Chem. 60 (1995) 2906–2908.
[6] (a) C.E. Henry, Q. Xu, Y.C. Fan, et al., J. Am. Chem. Soc. 136 (2014) 11890–11893;
(b) Z. Wang, T. Wang, W. Yao, Y. Lu, Org. Lett. 19 (2017) 4126–4129;
(c) T. Wang, Z. Yu, D.L. Hoon, et al., Chem. Sci. 6 (2015) 4912–4922;
(d) A.J. Smaligo, S. Vardhineedi, O. Kwon, ACS Catal. 8 (2018) 5188–5192;
(e) E. Li, H. Jin, P. Jia, X. Dong, Y. Huang, Angew. Chem. Int. Ed. 55 (2016) 11591–11594.
[7] H. Wang, X. Li, Y. Tu, J. Zhang, iScience 23 (2020) 101138.
[8] (a) H. Li, X. Hong, Chin. Chem. Lett. 29 (2018) 1585–1590;
(b) P.H.Y. Cheong, C.Y. Legault, J.M. Um, N. Çelebi-Ölçüm, K.N. Houk, Chem. Rev. 111 (2011) 5042–5137;
(c) C.X. Cui, C. Shan, Y.P. Zhang, et al., Chem. Asian J. 13 (2018) 1076–1088.
[9] (a) Y. Xia, Y. Liang, Y. Chen, et al., J. Am. Chem. Soc. 129 (2007) 3470–3471;
(b) H. Chen, L. Zhu, K. Zhong, et al., Chin. Chem. Lett. 29 (2018) 1237–1241;
(c) Y. Wang, Y. Lan, Chin. Chem. Lett. 31 (2020) 736–738;
(d) Y. Wang, M. Tang, Y. Wang, D. Wei, J. Org. Chem. 81 (2016) 5370–5380;
(e) T. Liu, S. Han, Y. Li, S. Bi, J. Org. Chem. 81 (2016) 9775–9784;
(f) Z. Yu, Z. Jin, M. Duan, et al., J. Org. Chem. 83 (2018) 9729–9740;
(g) B. Bhaskararao, G. Jindal, R.B. Sunoj, J. Org. Chem. 82 (2017) 13449–13458;
(h) G. Huang, C. Diner, K.J. Szabó, F. Himo, Org. Lett. 19 (2017) 5904–5907.
[10] (a) F.M. Bickelhaupt, K.N. Houk, Angew. Chem. Int. Ed. 56 (2017) 10070–10086;
(b) D.H. Ess, K.N. Houk, J. Am. Chem. Soc. 129 (2007) 10646–10647;
(c) X. Hong, Y. Liang, K.N. Houk, J. Am. Chem. Soc. 136 (2014) 2017–2025;
(e) S. Liu, Y. Lei, X. Qi, Y. Lan, J. Phys. Chem. A 118 (2014) 2638–2645;
(f) G. Huang, M. Kalek, R.Z. Liao, F. Himo, Chem. Sci. 6 (2015) 1735–1746;
(g) X. Zhang, H. Zou, G. Huang, ChemCatChem 8 (2016) 2549–2556;
(h) J. Yu, S. Zhang, X. Hong, J. Am. Chem. Soc. 139 (2017) 7224–7243;
(i) H. Wu, X. Li, X. Tang, C. Feng, G. Huang, J. Org. Chem. 83 (2018) 9220–9923;
(j) H. Zou, Z.L. Wang, Y. Cao, G. Huang, Chin. Chem. Lett. 29 (2018) 1355–1358.